



HAL
open science

Impaired aerobic capacity and premature fatigue preceding muscle weakness in the skeletal muscle Tfam KO mouse model

Benjamin Chatel, Sylvie Ducreux, Zeina Harhous, Nadia Bendridi, I. Varlet, Augustin C. Ogier, Monique Bernard, Julien Gondin, Jennifer Rieusset, Håkan Westerblad, et al.

► **To cite this version:**

Benjamin Chatel, Sylvie Ducreux, Zeina Harhous, Nadia Bendridi, I. Varlet, et al.. Impaired aerobic capacity and premature fatigue preceding muscle weakness in the skeletal muscle Tfam KO mouse model. *Disease Models & Mechanisms*, 2021, 14 (9), 10.1242/dmm.048981 . hal-03335080

HAL Id: hal-03335080

<https://hal.science/hal-03335080>

Submitted on 6 Sep 2021

HAL is a multi-disciplinary open access archive for the deposit and dissemination of scientific research documents, whether they are published or not. The documents may come from teaching and research institutions in France or abroad, or from public or private research centers.

L'archive ouverte pluridisciplinaire **HAL**, est destinée au dépôt et à la diffusion de documents scientifiques de niveau recherche, publiés ou non, émanant des établissements d'enseignement et de recherche français ou étrangers, des laboratoires publics ou privés.



Distributed under a Creative Commons Attribution 4.0 International License

Impaired aerobic capacity and premature fatigue preceding muscle weakness in the skeletal muscle *Tfam* KO mouse model

Benjamin Chatel^{1,2}, Sylvie Ducreux³, Zeina Harhous³, Nadia Bendridi⁴, Isabelle Varlet¹, Augustin C. Ogier⁵, Monique Bernard¹, Julien Gondin⁶, Jennifer Rieusset³, Håkan Westerblad⁷, David Bendahan¹, Charlotte Gineste^{1*}

¹ Aix-Marseille Univ, CNRS, CRMBM, Marseille, France

² CellMade, Le-Bourget-du-Lac, France

³ Univ Lyon, CarMeN Laboratory, INSERM, INRA, INSA Lyon, Université Claude Bernard Lyon 1, 69500, Bron, France

⁴ Univ Lyon, CarMeN Laboratory, INSERM, INRA, INSA Lyon, Université Claude Bernard Lyon 1, 69600, Oullins, France

⁵ Aix Marseille Univ, Université de Toulon, CNRS, LIS, Marseille, France

⁶ Institut NeuroMyoGène, UMR CNRS 5310 – INSERM U1217, Université Claude Bernard Lyon 1, Lyon, France

⁷ Department of Physiology and Pharmacology, Karolinska Institutet, 171 77 Stockholm, Sweden

***Corresponding Author:** Charlotte GINESTE; IGBMC, 1 Rue Laurent Fries, 67400 Illkirch, France. ginestec@igbmc.fr

ABSTRACT

Mitochondrial diseases are genetic disorders leading to an impaired mitochondrial function and resulting in exercise intolerance and muscle weakness. In patients, muscle fatigue due to defects in mitochondrial oxidative capacities commonly precedes muscle weakness. In mice, the fast-twitch skeletal muscle-specific *Tfam* deletion (*Tfam* KO) leads to deficit in the

respiratory chain activity, severe muscle weakness and early death. Here, we performed a time-course study of mitochondrial and muscular dysfunctions in 11 and 14 weeks *Tfam* KO mice, *i.e.*, before and when mice are about to enter the terminal stage, respectively. While force in the unfatigued state was reduced in *Tfam* KO mice as compared to control littermates (WT) only at 14 weeks, during repeated submaximal contractions fatigue was faster at both ages. During fatiguing stimulation, total phosphocreatine breakdown was larger in *Tfam* KO muscle than in WT muscle at both ages whereas phosphocreatine consumption was faster only at 14 weeks. In conclusion, the *Tfam* KO mouse model represents a reliable model of lethal mitochondrial myopathy where impaired mitochondrial energy production and premature fatigue occur before muscle weakness and early death.

KEY WORDS: mitochondrial myopathy, energy metabolism, muscle fatigue, exercise intolerance, muscle weakness

SUMMARY STATEMENT

Decreased resistance to fatigue together with decreased oxidative capacities arise ahead of muscle weakness in a mouse model of mitochondrial myopathy.

INTRODUCTION

Mitochondrial diseases are caused by genetic mutations in mitochondrial or nuclear DNA which affect the function of the mitochondrial respiratory chain thereby leading to a defective oxidative phosphorylation (Ishikawa and Nakada, 2020; Parikh et al., 2015; Thorburn, 2004). Skeletal muscles are commonly affected given that they require a high amount of energy and are highly dependent on oxidative phosphorylation for energy production. Clinical manifestations of mitochondrial myopathy generally include exercise

intolerance, muscle weakness, and muscle wasting (Petty et al., 1986). A main histological hallmark of mitochondrial myopathies is the presence of ragged-red fibers, which are muscle fibers exhibiting mitochondrial aggregates in subsarcolemmal regions (Milone and Wong, 2013).

The mitochondrial oxidative phosphorylation system consists of five multi-heteromeric complexes embedded in the inner mitochondrial membrane and composed of subunits encoded by both nuclear and mitochondrial DNA (except complex II which is only encoded by nuclear DNA) (Larsson and Oldfors, 2001; Rotig and Munnich, 2003). The mitochondrial transcription factor A (*Tfam*) encoded by nuclear DNA is a protein with a key role in mitochondrial DNA maintenance (Larsson et al., 1998). Disruption of *Tfam* has been shown to cause a global deficiency of all mitochondrial DNA-encoded proteins, hence affecting complexes I, III, IV, and V (Wredenberg et al., 2002).

The mouse model with a selective *Tfam* knockout in fast-twitch skeletal muscle fibers (*Tfam* KO) has been shown to mimic pathological features typically reported in patients with mitochondrial myopathies, including ragged-red fibers with abnormally positioned and enlarged mitochondria, atrophic fibers, COX-deficient fibers, and reduction of the respiratory chain enzyme activities (Aydin et al., 2009; Wredenberg et al., 2002). The *Tfam* KO mice do not live more than ~20 weeks and appear healthy until 12-14 weeks when a progressive clinical phenotype becomes evident (Gineste et al., 2015; Wredenberg et al., 2002). Experiments conducted in isolated whole muscles and intact single muscle fibers of *Tfam* KO mice aged of 12-14 weeks have shown muscle weakness (*i.e.*, lower muscle force production) associated with a prolonged and excessive mitochondrial calcium (Ca^{2+}) accumulation (Aydin et al., 2009; Gineste et al., 2015). However, muscle fatigue (*i.e.*, drop in force during sustained or repeated contractions) remained unaffected and has been explained by an increased proportion of the muscle fiber volume being occupied by mitochondria combined with a lower energy expenditure during contractions. This reduced cost would be due to a reduced sarcoplasmic reticulum (SR) calcium (Ca^{2+}) release resulting in a decreased activation of the energy-consuming cross-bridges and SR Ca^{2+} pumps (Aydin

et al., 2009; Wredenberg et al., 2002). A similar lack of effect on muscle fatigue has been previously demonstrated in nemaline myopathy mouse models that also display a severe muscle weakness (Gineste et al., 2013; Gineste et al., 2020) and might then be due to the fact that experiments have been conducted in relatively late stages of the disease, *i.e.*, when severe muscle weakness was established and the resulting energy consumption during contractions was decreased. Accordingly, premature fatigue (*i.e.*, faster drop in force) related to decreased mitochondrial oxidative capacity has been shown to precede overt muscle weakness in mouse models with mitochondrial dysfunction as well as in patients with mitochondrial myopathies (Finsterer, 2020; Tarnopolsky, 2016; Yamada et al., 2012).

In the present study, we hypothesized that faster muscle fatigue and impaired mitochondrial energy production precede muscle weakness in the *Tfam* KO mouse model. *In vivo* metabolic changes, force production and muscle fatigue were assessed in *Tfam* KO mice at two different time-points, *i.e.*, before mice enter the stage with obvious symptoms (*i.e.*, at 11 weeks) and when mice are about to enter the terminal stage with progressive muscle weakness (*i.e.*, at 14 weeks). These *in vivo* investigations of the skeletal muscle function were combined with *in vitro* experiments on isolated muscles to study whether there were structural alterations indicating increased mitochondrial Ca^{2+} influx via mitochondria-associated membranes (MAM) (Csordas et al., 2018), which might explain the excessive mitochondrial Ca^{2+} uptake observed in *Tfam* KO muscle fibers during repeated contractions (Aydin et al., 2009; Gineste et al., 2015).

RESULTS

Progressive body weight loss is associated with skeletal muscle atrophy without fatty replacement of muscle in Tfam KO mice

Skeletal muscle atrophy and replacement of skeletal muscle tissue by fat deposition or fibrotic tissue is a frequent feature in muscular disorders and has been reported in patients with mitochondrial myopathy, although it is not a common feature (Olsen et al., 2003;

Theodorou et al., 2012). Therefore, we measured body weight and hindlimb muscles volume using magnetic resonance imaging (MRI) in *Tfam* KO mice and their control littermates, which will be referred to as WT. We also determined whether muscle was replaced by fatty infiltration.

At 11 weeks of age, *Tfam* KO and WT mice had a similar body weight while at 14 weeks body weight was ~15% lower in *Tfam* KO than in WT mice (Fig. 1A). While no difference was observed between *Tfam* KO mice between the two ages, body weight was higher in WT mice at 14 weeks compared to 11 weeks.

The volume of hindlimb muscles was ~15% lower in *Tfam* KO than in WT mice at 14 weeks while no difference existed at 11 weeks (Fig. 1B and 1C), indicating muscle atrophy at 14 weeks in *Tfam* KO mice. No difference was observed between 11 weeks and 14 weeks for the two genotypes.

Neither intramuscular fatty infiltration nor fibrotic tissue was detected in *Tfam* KO mice at either age as illustrated by the absence pixels with higher intensities in the muscle region (Fig. 1C).

Reduced maximal force at 14 weeks in Tfam KO mice is related to muscle atrophy

Patients with mitochondrial myopathies usually present skeletal muscle weakness (*i.e.*, decreased force production) (Moggio et al., 2014), which is a common feature reported in neuromuscular diseases (Ahmed et al., 2018; Scelsi, 1992) and which may be due to skeletal muscle atrophy and/or impaired contractile function within the muscles. In order to determine whether the *Tfam* KO mice showed skeletal muscle weakness, we measured maximal force production (at 150 Hz) and submaximal force production (at 20 Hz that gives <50% of maximal force) in the unfatigued state. We assessed both absolute force and specific force, *i.e.*, force normalized to hindlimb muscle volume to assess contractile function independently of hindlimb muscle size.

Absolute maximal tetanic forces did not differ between *Tfam* KO and WT mice at 11 weeks whereas force was ~15% lower in *Tfam* KO mice at 14 weeks (Fig. 2A). When normalized to hindlimb muscles volume, force was similar in *Tfam* KO and WT mice at both ages, indicating that muscle weakness at 14 weeks in *Tfam* KO mice is related to muscle atrophy. No difference in maximal force was observed between 11 weeks and 14 weeks for the two genotypes. No significant difference was found for absolute and specific submaximal forces between groups for the same age. Nevertheless, both absolute and specific force at 20 Hz increased for WT mice between 11 and 14 weeks while no significant change was observed for *Tfam* KO mice (Fig. S1).

Faster fatigue in Tfam KO than in WT mice at 11 and 14 weeks

Premature muscle fatigue (*i.e.*, faster decline in force during sustained or repeated contractions) is a typical feature in patients with mitochondrial myopathy (Finsterer, 2020; Tarnopolsky, 2016). We measured force production during 80 repeated submaximal contractions (1.5 s contractions given every 7.5 s). Specific force was significantly decreased in *Tfam* KO mice from the 15th to 50th contraction at 14 weeks, whereas it was similar between the two groups at 11 weeks (Fig. 2B and 2C). Absolute force was significantly lower in *Tfam* KO than in WT mice from 25th to 35th contractions at 11 weeks and from 10th to 50th at 14 weeks (Fig. S2).

We performed two additional measurements to characterize changes in force production during fatiguing stimulation. First, the total specific force produced throughout the exercise period was similar between WT and *Tfam* KO mice at 11 weeks, while it was significantly reduced by ~35% at 14 weeks in *Tfam* KO mice as compared to WT mice (Fig. 2C). We also measured the contraction that gives 50% of the initial force (C_{50}) because the rate of decline in force differed largely in the initial part of fatiguing stimulation between *Tfam* KO and WT mice. The results revealed a markedly faster initial force decline (lower C_{50}) in *Tfam* KO than in WT mice at both ages (Fig. 2D) indicating that fatigue was faster in *Tfam* KO mice at both ages. It is worth noting that force reached a relatively stable low level

towards the end of fatiguing stimulation during which forces were similar in *Tfam* KO and WT mice (see Fig. 2B). One likely explanation for this is that towards the end of the stimulation period, force was maintained primarily by highly fatigue resistant slow-twitch muscle fibers, which are not genetically afflicted in the fast-twitch muscle fiber-specific *Tfam* KO mouse.

The muscle energetic status at rest is affected in Tfam KO mice at both ages

Patients with mitochondrial myopathy present impaired muscle metabolism at rest and particularly during exercise (Argov et al., 1987; Matthews et al., 1991; Radda et al., 1985; Taylor et al., 1994). Thus, we used phosphorus-31 magnetic resonance spectroscopy (³¹P-MRS) to study differences in energy metabolites at rest and during repeated contractions (Fig. 3A). At rest, [phosphocreatine] to [ATP] ratio was not significantly different between *Tfam* KO and WT mice at 11 weeks but significantly lower at 14 weeks (Fig. 3B). Resting [inorganic phosphate] was significantly higher in *Tfam* KO than in WT mice at both ages and this metabolic impairment in *Tfam* KO mice progressed between 11 and 14 weeks (Fig. 3C). Resting pH_i was not significantly different between groups at either 11 or 14 weeks (Fig. 3D). The increase in [inorganic phosphate] together with the reduced phosphocreatine] to [ATP] ratio at 14 weeks in *Tfam* KO mice indicate an impaired metabolic regulation with inadequate matching between oxidative ATP supply and demand in the resting state.

Impaired muscle energy metabolism during fatiguing contractions in Tfam KO mice at 11 and 14 weeks

We also investigated muscle bioenergetics during a standardized fatiguing exercise protocol through the time-course changes in [phosphocreatine], [inorganic phosphate] and pH_i. During a contractile activity, skeletal muscles require ATP produced by both anaerobic and oxidative metabolism. The major anaerobic ATP sources are breakdown of phosphocreatine, which results in accumulation of inorganic phosphate ions, and glycolysis ending with lactate and hydrogen ions (H⁺) formation. During the first 2 min of exercise, [phosphocreatine] decreased rapidly and then reached a stable low level at 5 min of

stimulation (Fig. 4A). The initial rate of phosphocreatine consumption was similar in *Tfam* KO and WT mice at 11 weeks, whereas it was ~70% higher in *Tfam* KO mice than in WT mice at 14 weeks (Fig. 4B). The magnitude of [phosphocreatine] depletion was significantly larger in the *Tfam* KO mice than in the WT mice at both 11 and 14 weeks (Fig. 4C). The increase in [inorganic phosphate] evolved as a mirror of [phosphocreatine], *i.e.*, inorganic phosphate levels increased rapidly during the first 2 minutes of exercise followed by a plateau from 5 min to the end of the stimulation period (Fig. 4D & 4E). An increased cytosolic inorganic phosphate levels are considered to be a major cause of force decline in skeletal muscle fatigue (Westerblad and Allen, 1996). Having this in mind, we plotted the relation between force and [inorganic phosphate] after 2.5 min of fatiguing stimulation (*i.e.*, covering the part of fatiguing stimulation where both these parameters showed rapid changes) for individual mice at 11 and 14 weeks (Fig. 4F) and found a strong significant negative correlation between these two variables ($r=-0.69$; $P<0.001$).

The decrease in pH_i during the fatiguing stimulation was similar in *Tfam* KO and WT mice with the only exception being a significant less acidosis at 5 min of stimulation in *Tfam* KO than in WT mice at 14 weeks (Fig. 4G). Decreased pH_i is commonly considered as a major cause of force decline in fatigued skeletal muscle, although its role is currently debated (Westerblad, 2016). Plotting the relation between force and pH_i after 2 min of fatiguing stimulation did not show any significant correlation ($r=-0.01$; $P=0.93$; Fig. 4H).

Slowed recovery kinetics of [phosphocreatine] in Tfam KO mice at 11 and 14 weeks

Phosphocreatine recovery kinetics are related to the end-exercise rate of oxidative ATP synthesis and a slowed phosphocreatine recovery has been recognized as indicative of an impaired mitochondrial oxidative function (Arnold et al., 1984), and a slower rate has been commonly reported in patients with mitochondrial myopathies (Barbiroli et al., 1997; Bendahan et al., 1992; Taylor et al., 1994). We evaluated the recovery time-courses of both phosphocreatine and inorganic phosphate for 10 min after the end of the fatiguing protocol (see Fig. 4A and 4B). The initial rate of phosphocreatine recovery was significantly lower in

Tfam KO than in WT mice at both 11 and 14 weeks (Fig. 5A). Likewise, at both ages the time constant of phosphocreatine recovery (T_{PCr}) was significantly longer in the *Tfam* KO than in WT mice at both ages (Fig. 5B) and [phosphocreatine] was still ~15% lower in *Tfam* KO than in WT mice at the end of the 10 min recovery period (Fig. 5C, Table S1). Additionally, [phosphocreatine] was not fully returned to resting levels after the 10min of recovery in *Tfam* KO mice (Fig. 4A, Table S1). The decrease in [inorganic phosphate] during recovery followed the same time course and was significantly higher in *Tfam* KO than in WT mice at the end of the recovery period at both ages (Fig. 5D). Moreover, [inorganic phosphate] at the end of the recovery period was significantly higher than the resting level in *Tfam* KO mice (Fig. 4D, Table S1). During the post-stimulation recovery period, pH_i gradually increased towards its resting level at a similar rate in *Tfam* KO and WT mice (Fig. 4G).

The contact points at the MAM level are decreased in Tfam KO muscle

To study whether alterations in MAM might be involved in the excessive mitochondrial Ca^{2+} uptake in *Tfam* KO muscle fibers (Aydin et al., 2009; Gineste et al., 2015), mitochondria and MAM were isolated from gastrocnemius muscles of 14 weeks WT and *Tfam* KO mice. No statistically significant difference between WT and *Tfam* KO mice was observed for the MAM protein content related to muscle weight (Fig. 6A) or isolated mitochondria (Fig. 6B), or for total mitochondrial protein content related to muscle weight (Fig. 6C). The physical SR-mitochondria interaction, assessed as the *in situ* protein-protein interaction between the SR Ca^{2+} channel inositol 1,3,4-triphosphate receptor 1 (IP₃R1) and the mitochondrial outer membrane voltage-dependent anion channel 1 (VDAC1) (Szabadkai et al., 2006), was significantly lower in *Tfam* KO than in WT mice (Fig. 6D).

DISCUSSION

In this study, we used a mouse model of lethal mitochondrial myopathy, the fast-twitch skeletal muscle-specific *Tfam* KO mouse. Experiments were performed at an early state of the disease process and our results show an impaired mitochondrial energy production accompanied by a faster force decline during repeated contractions in *Tfam* KO than in WT mice; these impairments occurred before any signs of reduced hindlimb muscle volume and decreased force production in the unfatigued state. In other words, muscles of *Tfam* KO mice showed an increased muscle fatigue before entering the state with progressive muscle atrophy and muscle weakness. These results extend those from previous studies showing a severe muscle weakness in more advanced stages of the disease (Gineste et al., 2015; Wredenberg et al., 2002) and support those reported in patients related to a progression from early premature fatigue to disabling muscle weakness already at rest (Finsterer, 2020; Tarnopolsky, 2016).

Contractile function in the unfatigued state was impaired in *Tfam* KO mice only at 14 weeks and at maximal force and was directly related to the skeletal muscle atrophy occurring at this age as normalized force was not different from that in WT mice. The absence of muscle weakness independently from muscle atrophy at maximal and submaximal forces contrasts with previous results showing a ~20% reduction in the force produced by isolated single fast-twitch muscle fibers of *Tfam* KO mice tested at a similar stage of the disease process, which was related to decreased SR Ca^{2+} release (Aydin et al., 2009). This apparent difference might be due to the fact that *in vivo* the decreased muscle fiber force production might be compensated by various non-contractile structures contributing to force transmission which are partly missing in experiments on isolated single fibers (Cornwall, 1984; Ward et al., 2020). A decreased force production in fast-twitch muscle fibers of *Tfam* KO mice might also be masked in the present *in vivo* experiments by a substantial proportion of the muscle being occupied by normally contracting slow-twitch fibers in which *Tfam* was not knocked out (Wredenberg et al., 2002). In this context it can be noted that the maintained low force levels observed towards the end of fatiguing stimulation likely reflect sustained

force production in fatigue resistant slow-twitch fibers. Accordingly, these maintained low force levels were of similar size in *Tfam* KO and WT mice, which fits with the normal genetic status of slow-twitch fibers in our *Tfam* KO mouse model.

Conversely, muscle fatigue induced by repeated submaximal contractions developed markedly faster at both 11 and 14 weeks in *Tfam* KO mice when compared to WT mice, but was associated with reduced force production in the unfatigued state only at 14 weeks. This result highlights that accelerated muscle fatigue precedes muscle weakness in *Tfam* KO mice. The altered muscle fatigue was particularly marked in the initial part of fatiguing stimulation. This early undue fatigue in the *Tfam* KO mice clearly mirrors the exercise intolerance commonly observed in patients with mitochondrial myopathy (Taivassalo and Haller, 2005; Taivassalo et al., 2003). Accelerated fatigue during repeated tetanic stimulation was not previously reported in single muscle fibers isolated from *Tfam* KO mice at a similar stage in the disease process (Aydin et al., 2009). Three differences between the present and the previous study might explain this discrepancy. First, tetanic force and free cytosolic $[Ca^{2+}]_i$ were already reduced at the start of fatiguing stimulation in the previous single fiber experiments. This means that less energy was used for cross-bridge cycling and SR Ca^{2+} reuptake during contractions and hence the stress on mitochondrial energy production was lowered, which would slow fatigue development (Cheng et al., 2019). Second, fatigue was induced by repeated submaximal (~50% of the maximal force) contractions in the present study, whereas close to maximal (~85% of the maximal force) contractions were used in the previous single fiber study. Submaximal contractions are on the steep part of the force- $[Ca^{2+}]_i$ relationship where fatigue-induced decreases in tetanic $[Ca^{2+}]_i$ and myofibrillar Ca^{2+} sensitivity have a much larger impact than with near-maximal contractions (Allen et al., 2008; Place et al., 2010). Third, the knockout of *Tfam* in fast-twitch skeletal muscle fibers might cause additional maladaptive modifications that limit *in vivo* fatigue but have no direct impact on the fatigue of isolated muscle fibers. For instance, slower heart rate kinetics at the onset of exercise have been observed in mitochondrial myopathy patients (Grassi et al., 2009).

Our results show clear-cut signs of impaired intracellular energy metabolism before, during and after the fatiguing stimulation bout in *Tfam* KO muscles at 11 and 14 weeks, which is consistent with the impaired mitochondrial oxidative metabolism observed in mitochondrial myopathy patients (Arnold et al., 1985; Hayes et al., 1985; Matthews et al., 1991; Moller et al., 2005; Taylor et al., 1994). In the resting state, *Tfam* KO muscles displayed a progressive increase in [inorganic phosphate], which would be required to maintain an adequate rate of mitochondrial ATP synthesis as mitochondrial function declines (Wu et al., 2007).

During the fatiguing protocol, phosphocreatine breakdown was larger in *Tfam* KO mice at both ages and faster in the initial part of the exercise at 14 weeks. These changes in [phosphocreatine] were mirrored by an increase in [inorganic phosphate] and indicate an increased dependency on phosphocreatine hydrolysis to maintain ATP levels during repeated contractions. Moreover, we observed a good correlation between the increase in [inorganic phosphate] and the decrease in force during the stimulation period (see Fig. 4F), which fits with inorganic phosphate being a major causative factor in acute muscle fatigue that afflicts cross-bridge force production, myofibrillar Ca^{2+} sensitivity and SR Ca^{2+} release (Allen et al., 2008).

In addition to phosphocreatine breakdown, the major anaerobic energy source is glycolysis ending with formation of lactate and H^+ when coupled to ATP hydrolysis. Intramuscular acidosis has not been reported as a distinctive characteristic of mitochondrial diseases (Arnold et al., 1985; Hayes et al., 1985; Taylor et al., 1994). Accordingly, resting pH_i was unaltered in *Tfam* KO mice at both ages and so in agreement with reports from patients with mitochondrial myopathies (Arnold et al., 1985; Hayes et al., 1985; Moller et al., 2005). Moreover, we observed no difference in pH_i changes during exercise and recovery periods between *Tfam* KO and WT mice except for a slightly larger acidification at 5 min of stimulation in WT mice at 14 weeks. These results imply that the faster fatigue in *Tfam* KO muscle is independent of acidosis. This implication is emphasized by the lack of correlation between decreased pH_i and reduced force during fatiguing stimulation (see Fig. 4H) and fits

with previous results demonstrating that acidosis is not the primary cause of exercise intolerance in patients with mitochondrial myopathy (Vissing et al., 2001).

Finally, a larger PCr consumption together with a similar or a lower force production (11 weeks and 14 weeks, respectively) might reflect a higher energy cost of contraction. It can be noted that during the first minute of fatiguing stimulation, where ATP production relies on anaerobic processes in both *Tfam* KO and WT muscles (Lannergren and Westerblad, 1991), the rate of force decline was similar in *Tfam* KO and WT muscles (see Fig. 4B). Thereafter, when aerobic ATP production becomes increasingly more important, fatigue developed at a faster rate in *Tfam* KO than in WT muscles. These results imply that the accelerated fatigue development in *Tfam* KO muscle is due to impaired mitochondrial oxidative capacity rather than increased energy cost of contraction, but further experiments directly addressing this issue are needed to provide a solid answer to this question.

The post-stimulation recovery kinetics of [phosphocreatine] can be used as an index of the mitochondrial oxidative capacity *in vivo* (Arnold et al., 1984; Lanza et al., 2011). The rate of [phosphocreatine] recovery was markedly decreased and the 10 min recovery period was not long enough for a complete recovery *Tfam* KO mice, which is in agreement with the slow [phosphocreatine] recovery kinetics commonly reported in patients with mitochondrial myopathies (Barbiroli et al., 1997; Bendahan et al., 1992; Kornblum et al., 2005; Moller et al., 2005; Radda et al., 1982; Taylor et al., 1994). Intriguingly, the slowing of [phosphocreatine] recovery was similar in 11 and 14 weeks *Tfam* KO mice thereby suggesting that the decline in mitochondrial oxidative capacity was not progressing within this time frame. This is in contrast to the faster initial decrease in [phosphocreatine] during induction of fatigue at 14 weeks than at 11 weeks. Lower [phosphocreatine] in muscle of exercising humans has been linked to reduced oxygen supply (Haseler et al., 2004) and slower pulmonary O₂ uptake and heart rate kinetics at the onset of moderate-intensity exercise has been observed in mitochondrial myopathy patients (Grassi et al., 2009). Thus, the faster initial rate of phosphocreatine consumption during exercise in the *Tfam* KO mice at 14 weeks, as well as

in mitochondrial myopathy patients, appears to involve factors other than the decrease in mitochondrial oxidative capacity in skeletal muscle.

Excessive Ca^{2+} accumulation in mitochondria during contraction has been suggested to be a main causative factor of muscle weakness in *Tfam* KO mice (Aydin et al., 2009) and the SR-mitochondria interface has been proposed to be the Ca^{2+} entry site (Gineste et al., 2015). Indeed, MAM can allow Ca^{2+} fluxes from the SR to mitochondria and thereby speed up mitochondrial respiration (Csordas et al., 2018). The present results show similar amount of MAM in *Tfam* KO and WT muscle, whereas the number of contact points between VDAC in the outer mitochondrial membrane and the SR Ca^{2+} channel $\text{IP}_3\text{R1}$ was lower in *Tfam* KO muscle. Obviously, the reduced number of VDAC- $\text{IP}_3\text{R1}$ contact points cannot explain the excessive mitochondrial Ca^{2+} uptake in *Tfam* KO muscle. Importantly, the aberrant mitochondrial Ca^{2+} accumulation in *Tfam* KO muscle fibers occurs during repeated contractions where SR Ca^{2+} release is mediated via another Ca^{2+} channel, the ryanodine receptor 1 (Hernandez-Ochoa and Schneider, 2018; Santulli et al., 2017; Shishmarev, 2020). Furthermore, on the mitochondrial side, the MAM-related matrix protein cyclophilin D (also called peptidyl-prolyl cis-trans isomerase F) is involved in the excessive Ca^{2+} uptake as illustrated by results showing (i) partial inhibition of the uptake by application of the cyclophilin D-binding inhibitor cyclosporine A, (ii) an increased protein expression of cyclophilin D in skeletal muscle from both *Tfam* KO mice and mitochondrial myopathy patients, and (iii) an increased life-span of cyclosporine A-treated *Tfam* KO mice (Aydin et al., 2009; Gineste et al., 2015). Thus, the contraction-mediated aberrant mitochondrial Ca^{2+} accumulation in *Tfam* KO muscle is unlikely to occur via VDAC- $\text{IP}_3\text{R1}$ -dependent interactions, but a role of MAM that involves ryanodine receptor 1-cyclophilin D interactions cannot be excluded.

Although the present *Tfam* KO mouse model mimics major features of human mitochondrial myopathies, it also has limitations. For instance, *Tfam* is knocked out only in fast-twitch muscle fibers so that there are still intact slow-twitch fibers that may disguise functional impairments and this differs from patients with mitochondrial myopathy where

mutations affect all muscle fiber types. Moreover, mitochondrial mutations in humans will be present in various cell types and functional impairments can be seen in other organs than skeletal muscle. Finally, *Tfam* KO mice show a rapidly progressing myopathy with only a few weeks between the first overt symptoms and death, which makes investigations in the later stage of the disease cumbersome.

In conclusion, disorders related to an impaired mitochondrial function are highly diverse and complex with different organs being affected in a rather unpredictable manner. Numerous mouse models have been generated to better understand the pathogenic mechanisms underlying mitochondrial diseases (Ishikawa and Nakada, 2020). In this study we used fast-twitch muscle fiber-specific *Tfam* KO mice and showed that this mouse model presents a disease progression similar to that observed in mitochondrial myopathy patients; that is, an initial decline in mitochondrial oxidative capacity accompanied by a faster force decline during repeated contractions (*i.e.*, accelerated development of muscle fatigue), which is followed by a progressive decrease in force production already in the unfatigued state (*i.e.*, muscle weakness), reduction of body weight and premature death. Thus, the present *Tfam* KO mice provide a good model for studies of mechanisms underlying muscle defects at different stages of mitochondrial myopathies and the knowledge gained can be used to propose novel treatment strategies for these serious diseases where no effective treatment currently exists.

MATERIALS AND METHODS

Animals

Tfam KO mice and their control littermates (referred to as WT) were used for experiments. The fast-twitch skeletal muscle fiber-specific *Tfam* KO mouse model was generated as previously described (Wredenberg et al., 2002). A first group of mice was tested at 11 weeks of age (*i.e.*, before mice enter the stage with severe phenotype) and a second group at 14 weeks of age (*i.e.*, when mice are about to enter the terminal stage with

weight loss and a marked reduction in force production) (Wredenberg et al., 2002). All experiments were conducted in agreement with the French guidelines for animal care and in conformity with the European convention for the protection of vertebrate animals used for experimental purposes and institutional guidelines n° 86/609/CEE November 24, 1986. All animal experiments were approved by the Institutional Animal Care Committee of Aix-Marseille University (permit number: #12522-2017121119249655 v1). Mice were housed in an environment-controlled facility (12–12 h light-dark cycle, 22 °C) and received water and standard food *ad libitum*.

Study design

Functional, anatomical and metabolic investigations of the left hindlimb muscles of WT and *Tfam* KO mice were performed strictly non-invasively *in vivo*. Body weight was measured before mice were subjected to the following protocol. The mechanical performance was assessed by measuring plantar flexor muscles (*gastrocnemius* [Gas], *soleus* [Sol], and *plantaris*) maximal tetanic force, and plantar flexor muscles force production during a fatiguing protocol. Metabolic changes were evaluated before, during, and after the fatiguing stimulation protocol using phosphorus-31 magnetic resonance spectroscopy (³¹P-MRS). Before the fatiguing protocol, the volume of hindlimb muscles was quantified by magnetic resonance imaging (MRI). Mice were euthanized by cervical dislocation at the end of the force and MR experiments.

Animal preparation

Mice were initially anesthetized in an induction chamber (Equipement vétérinaire; Minerve, Esternay, France) with 4% isoflurane in 33% O₂ (0.5 L/min) and 66% N₂O (1 L/min) and placed supine in a cradle designed in our laboratory. A custom-built facemask continuously supplied with 1.75% isoflurane in 33% O₂ (0.2 L/min) and 66% N₂O (0.4 L/min) was incorporated into the cradle and was used to maintain a prolonged anesthesia throughout the experiment. The hindlimb was centered inside a 16 mm-diameter ¹H

Helmholtz imaging coil and the belly of the Gas muscle was located above an elliptical (6 x 8 mm) ^{31}P -MRS surface coil. The foot was positioned on the pedal of a custom-made ergometer with a 90° flexion ankle joint. A force transducer was part of the pedal as previously described (Giannesini et al., 2010). Two rod-shaped surface electrodes integrated into the cradle and connected to an electrical stimulator (Digitimer, Ltd., Model DS7A, Welwyn Springs, UK) were placed on the left hindlimb, one at the heel level and the other one just above the knee joint.

Force output measurements

The analog electrical signal coming out from the force transducer was amplified with a home-built amplifier (Operational amplifier AD620; Analog Devices, Norwood, MA, USA), converted to a digital signal, monitored and recorded on a personal computer using the Powerlab 35/series system (AD Instruments, Oxford, United Kingdom). Skeletal muscle contractions were achieved by non-invasive transcutaneous electrical stimulation elicited with square-wave pulses (0.5 ms duration). The individual maximal stimulation intensity was determined by progressively increasing the stimulus intensity until there was no further increase in peak twitch force. Maximal tetanic force of the plantar flexor muscles was assessed in response to a 150 Hz pulse train (duration = 0.75 s) and submaximal force in response to 20 Hz (duration = 0.75 s). Plantar flexor muscles force production was also measured during a fatigue protocol (80 contractions - 40 Hz - 1.5 s on, 6 s off).

The peak force of each contraction was measured with the LabChart software (AD Instruments, Oxford, United Kingdom). Regarding the fatigue protocol, the tetanic force was averaged every 5 contractions for the sake of clarity. The total force production was computed as the sum of each individual peak force measured during the fatigue protocol. The C_{50} corresponded to the contraction number at which the force amplitude was 50% of the initial force of the fatiguing exercise. Force was normalized with respect to the volume of hindlimb muscles (see below) to obtain specific force (in mN/mm^3).

MR experiments

Investigations were performed with a 47/30 Biospec Avance MR system (Bruker, Karlsruhe, Germany) equipped with a 120-mm BGA12SL (200 mT/m) gradient insert.

Anatomical imaging

MRI data were acquired at rest, *i.e.*, before fatiguing protocol. Fifteen consecutive contiguous axial slices (thickness = 0.7 mm), covering the region from the knee to the ankle, were selected across the lower hindlimb. Rapid acquisition with relaxation enhancement (RARE) images (rare factor = 4, effective echo time = 22.5 ms, actual echo time = 10.6 ms, repetition time = 1000 ms, number of averages = 10, number of repetition = 1, pulse type = hermite, pulse duration = 2 ms, flip angle = 90°, sweep width, 2.7 kHz, field of view = 4.2×4.2 cm, matrix size = 256×192 and acquisition time = 8 min 00 s) were recorded.

Images were analyzed with FSLview (FMRIB, Oxford, MS) (Jenkinson et al., 2012). The border of the whole hindlimb muscle area was manually delineated in the two slices located on the proximal and distal parts. Segmentation of the missing intermediate slices was automatically performed on the basis of image registration procedures as previously described (Ogier et al., 2017). The volume of the hindlimb muscles (mm³) was calculated as the sum of the volume of the ten consecutive largest slices, which were located on the proximal part and covered the largest volume of the hindlimb muscle belly.

Metabolism

³¹P spectra (8-kHz sweep width; 2048 data points) from the posterior hindlimb muscles region were acquired continuously throughout the standardized rest – fatigue – recovery protocol. A total of 800 partially saturated (repetition time = 2 s) free induction decays (FID) were recorded.

³¹P-MRS data were processed using a proprietary software developed using IDL (Interactive Data Language, Research System, Inc., Boulder, CO, USA) (Le Fur et al., 2010). The first 180 FID were acquired at rest and summed together (n = 1, time resolution = 6 min). The next 320 FID were acquired during the stimulation period and summed by blocks of 80 during the stimulation procedure (n = 4, time resolution = 160 s). The last 300 FID were acquired during the recovery period and summed by blocks of 50 (n = 6, time resolution = 100 s). The relative concentrations of high-energy phosphate metabolites (phosphocreatine, inorganic phosphate and adenosine triphosphate (ATP)) were obtained by a time-domain fitting routine using the AMARES-MRUI Fortran code and appropriate prior knowledge of the ATP multiplets. As previously suggested (Chance et al., 1981), inorganic phosphate values were normalized to the sum of phosphocreatine and inorganic phosphate values, which were considered as constant in order to take into account potential movement artifacts. Intracellular pH (pH_i) was calculated from the chemical shift of the inorganic phosphate signal relative to phosphocreatine (Moon and Richards, 1973). The resting [phosphocreatine] to [ATP] ratio was calculated from the peak areas of the phosphocreatine and β-ATP of the spectrum acquired at rest. The initial rate of phosphocreatine degradation (rate of phosphocreatine degradation at the start of exercise; V_{i Phosphocreatine degradation}) was calculated as:

$$V_{i \text{ Phosphocreatine degradation}} = \Delta \text{Phosphocreatine}_{\text{degradation}} / \tau \text{Phosphocreatine}_{\text{degradation}},$$

where $\Delta \text{Phosphocreatine}_{\text{degradation}}$ is the percentage of phosphocreatine depletion measured at the exercise end (relative to basal value) and $\tau \text{Phosphocreatine}_{\text{degradation}}$ is the time constant of phosphocreatine degradation which was determined by fitting the time course of [phosphocreatine] level to a mono-exponential function with a least-mean-squared algorithm. Similarly, the phosphocreatine recovery kinetic parameters (initial rate of phosphocreatine resynthesis at the start of the recovery period (V_{i Phosphocreatine resynthesis}) and [phosphocreatine]

recovery time constant ($T_{\text{Phosphocreatine}}$) were determined during the post exercise period by fitting the time course of phosphocreatine resynthesis to a mono-exponential function.

Isolation of mitochondria-associated membranes (MAM)

Mice were euthanized by cervical dislocation and Gas muscles were extracted and immediately placed in Isolation Buffer, IB1, (225 mM mannitol, 75 mM sucrose, 0.5% BSA, 0.5 mM EGTA and 30 mM Tris HCl pH7.4) as previously described (Wieckowski et al., 2009). The tissues were finely minced with scissors and the pieces were then homogenized by applying 10-20 strokes in a glass-Teflon tissue grinder. The homogenates were centrifuged at 740 g for 5 min, and the supernatants were taken and similarly centrifuged. The new supernatants were collected and centrifuged at 9,000 g for 10 min at 4°C. The pellets were gently resuspended in a Stop Buffer, SB, (225 mM mannitol, 75 mM sucrose, 30 mM Tris-HCl pH 7.4) and centrifuged at 10,000 g for 10 min. The pellets of crude mitochondria were resuspended in Mitochondria Resuspending Buffer (MRB; 250 mM mannitol, 5 mM HEPES (pH 7.4) and 0.5 mM EGTA). For purifying mitochondria and MAM, the crude mitochondrial fractions were layered on top of Percoll medium (225 mM mannitol, 25 mM HEPES, 1 mM EGTA and 30 % Percoll (vol/vol) in 14 ml thin-wall Beckman ultracentrifugation tubes. MRB was added on top of the mitochondrial suspensions to fill up the tubes. The latter were centrifuged at 95,000 g for 30 min at 4°C. The MAM, identified as a round white layer in the middle of the tube, were collected and washed by MRB through centrifugation at 6,300 g /10 min/4 °C and then re-centrifuged in polycarbonate tubes using a 100,000 g/1h/4 °C ultracentrifugation. The ring of MAM at the bottom of the tubes was finally collected. Protein concentration was quantified by the Lowry method.

In Situ Proximity Ligation Assay

VDAC1 (ab14734) and IP₃R1 (sc28614) proximity were measured by *in situ* proximity ligation assay (PLA) (Sigma Duolink kits anti-rabbit plus (DUO92002) and anti-Mouse minus (DUO92004) to detect and quantify SR-mitochondria interactions, as previously described and thoroughly validated (Tubbs and Rieusset, 2016; Tubbs et al., 2014). In muscle tissue, *in situ* PLA were performed on paraffin-embedded sections, after an antigen retrieval at pH 6, using a bright-field revelation. Dots were quantified using Image J. Results were expressed as number of dots per field. A minimum of 10 images per muscle were analyzed.

Statistical analysis

Data are presented as mean \pm SEM. Statistical analyses were performed with GraphPad Prism software version 7.04. Normality was checked using a Shapiro-Wilk test. Parametric tests were performed when data were normally distributed. If not, non-parametric tests were used. Student's unpaired t-test or unpaired Mann-Whitney test was used to compare VDAC-IP3R1 interaction and MAM, respectively. Two-way ANOVA (genotype x age) was used to compare WT-11w, *Tfam* KO-11w mice, WT-14w and *Tfam* KO-14w mice. Two-way ANOVA with repeated measures on time or contraction number was used to compare force production or metabolic changes during induction of fatigue and recovery in the four groups. When a significant interaction was found, Tukey's post-hoc test was performed. When a main effect was found, Sidak's post-hoc test was performed. Statistical significance was accepted when $P < 0.05$. For the sake of clarity, when an interaction was found, we only show significant differences between: WT and *Tfam* KO mice at either 11 or 14 weeks; 11 weeks and 14 weeks for either WT or *Tfam* KO mice (*i.e.*, statistical differences between WT at 11 weeks vs. *Tfam* KO at 14 weeks and WT at 14 weeks vs. *Tfam* KO at 11 weeks are not shown).

ACKNOWLEDGEMENTS

This work was funded by the AFM-Téléthon (trampoline grant #19963 to CG). CRMBM is member of France Life Imaging network (grant ANR-11-INBS-0006).

AUTHOR CONTRIBUTIONS

CG conceived the project. BC and CG performed *in vivo* experiments. BC, IV, AO, CG analyzed the *in vivo* data. SD and ZH performed the MAM experiments and analyses. NB, SD and JR performed the PLA experiments and analyses. CG and BC wrote the manuscript. SD, MB, JG, HW, DB edited the manuscript. CG and DB supervised the work.

COMPETING INTERESTS

The authors declare no competing interests.

REFERENCES

- Ahmed, S. T., Craven, L., Russell, O. M., Turnbull, D. M. and Vincent, A. E.** (2018). Diagnosis and Treatment of Mitochondrial Myopathies. *Neurotherapeutics* **15**, 943-953.
- Allen, D. G., Lamb, G. D. and Westerblad, H.** (2008). Skeletal muscle fatigue: cellular mechanisms. *Physiol Rev* **88**, 287-332.
- Argov, Z., Bank, W. J., Maris, J., Peterson, P. and Chance, B.** (1987). Bioenergetic heterogeneity of human mitochondrial myopathies: phosphorus magnetic resonance spectroscopy study. *Neurology* **37**, 257-262.

Arnold, D. L., Matthews, P. M. and Radda, G. K. (1984). Metabolic recovery after exercise and the assessment of mitochondrial function in vivo in human skeletal muscle by means of ^{31}P NMR. *Magn. Reson. Med.* **1**, 307-315.

Arnold, D. L., Taylor, D. J. and Radda, G. K. (1985). Investigation of human mitochondrial myopathies by phosphorus magnetic resonance spectroscopy. *Ann. Neurol.* **18**, 189-196.

Aydin, J., Andersson, D. C., Hanninen, S. L., Wredenberg, A., Tavi, P., Park, C. B., Larsson, N. G., Bruton, J. D. and Westerblad, H. (2009). Increased mitochondrial Ca^{2+} and decreased sarcoplasmic reticulum Ca^{2+} in mitochondrial myopathy. *Hum. Mol. Genet.* **18**, 278-288.

Barbiroli, B., Frassinetti, C., Martinelli, P., Iotti, S., Lodi, R., Cortelli, P. and Montagna, P. (1997). Coenzyme Q10 improves mitochondrial respiration in patients with mitochondrial cytopathies. An *in vivo* study on brain and skeletal muscle by phosphorous magnetic resonance spectroscopy. *Cell. Mol. Biol.* **43**, 741-749.

Bendahan, D., Desnuelle, C., Vanuxem, D., Confort-Gouny, S., Figarella-Branger, D., Pellissier, J. F., Kozak-Ribbens, G., Pouget, J., Serratrice, G. and Cozzone, P. J. (1992). ^{31}P NMR spectroscopy and ergometer exercise test as evidence for muscle oxidative performance improvement with coenzyme Q in mitochondrial myopathies. *Neurology* **42**, 1203-1208.

Chance, B., Eleff, S., Leigh, J. S., Jr., Sokolow, D. and Sapega, A. (1981). Mitochondrial regulation of phosphocreatine/inorganic phosphate ratios in exercising human muscle: a gated ^{31}P NMR study. *Proc. Nat. Acad. Sci. U S A* **78**, 6714-6718.

Cheng, A. J., Hwee, D. T., Kim, L. H., Durham, N., Yang, H. T., Hinken, A. C., Kennedy, A. R., Terjung, R. L., Jasper, J. R., Malik, F. I. et al. (2019). Fast skeletal muscle troponin activator CK-2066260 increases fatigue resistance by reducing the energetic cost of muscle contraction. *J. Physiol.* **597**, 4615-4625.

Cornwall, M. W. (1984). Biomechanics of noncontractile tissue. A review. *Phys. Ther.* **64**, 1869-1873.

Csordas, G., Weaver, D. and Hajnoczky, G. (2018). Endoplasmic Reticulum-Mitochondrial Contactology: Structure and Signaling Functions. *Trends Cell Biol* **28**, 523-540.

Finsterer, J. (2020). Update Review about Metabolic Myopathies. *Life (Basel)* **10**.

Giannesini, B., Vilmen, C., Le Fur, Y., Dalmaso, C., Cozzone, P. J. and Bendahan, D. (2010). A strictly noninvasive MR setup dedicated to longitudinal studies of mechanical performance, bioenergetics, anatomy, and muscle recruitment in contracting mouse skeletal muscle. *Magn. Reson. Med.* **64**, 262-270.

Gineste, C., Hernandez, A., Ivarsson, N., Cheng, A. J., Naess, K., Wibom, R., Lesko, N., Bruhn, H., Wedell, A., Freyer, C. et al. (2015). Cyclophilin D, a target for counteracting skeletal muscle dysfunction in mitochondrial myopathy. *Hum. Mol. Genet.* **24**, 6580-6587.

Gineste, C., Le Fur, Y., Vilmen, C., Le Troter, A., Pecchi, E., Cozzone, P. J., Hardeman, E. C., Bendahan, D. and Gondin, J. (2013). Combined MRI and ³¹P-MRS investigations of the *ACTA1*(H40Y) mouse model of nemaline myopathy show impaired muscle function and altered energy metabolism. *PLoS One* **8**, e61517.

Gineste, C., Ogier, A. C., Varlet, I., Hourani, Z., Bernard, M., Granzier, H., Bendahan, D. and Gondin, J. (2020). In vivo characterization of skeletal muscle function in nebulin-deficient mice. *Muscle Nerve* **61**, 416-424.

Grassi, B., Porcelli, S., Marzorati, M., Lanfranconi, F., Vago, P., Marconi, C. and Morandi, L. (2009). Metabolic myopathies: functional evaluation by analysis of oxygen uptake kinetics. *Med. Sci. Sports Exerc.* **41**, 2120-2127.

Haseler, L. J., Kindig, C. A., Richardson, R. S. and Hogan, M. C. (2004). The role of oxygen in determining phosphocreatine onset kinetics in exercising humans. *J. Physiol.* **558**, 985-992.

Hayes, D. J., Hilton-Jones, D., Arnold, D. L., Galloway, G., Styles, P., Duncan, J. and Radda, G. K. (1985). A mitochondrial encephalomyopathy. A combined ³¹P magnetic resonance and biochemical investigation. *J. Neurol. Sci.* **71**, 105-118.

Hernandez-Ochoa, E. O. and Schneider, M. F. (2018). Voltage sensing mechanism in skeletal muscle excitation-contraction coupling: coming of age or midlife crisis? *Skelet Muscle* **8**, 22.

Ishikawa, K. and Nakada, K. (2020). Attempts to understand the mechanisms of mitochondrial diseases: The reverse genetics of mouse models for mitochondrial disease. *Biochim Biophys Acta Gen Subj* **1865**, 129835.

Jenkinson, M., Beckmann, C. F., Behrens, T. E., Woolrich, M. W. and Smith, S. M. (2012). *Fsl. Neuroimage* **62**, 782-790.

Kornblum, C., Schroder, R., Muller, K., Vorgerd, M., Eggers, J., Bogdanow, M., Papassotiropoulos, A., Fabian, K., Klockgether, T. and Zange, J. (2005). Creatine has no beneficial effect on skeletal muscle energy metabolism in patients with single mitochondrial DNA deletions: a placebo-controlled, double-blind ³¹P-MRS crossover study. *Eur. J. Neurol.* **12**, 300-309.

Lannergren, J. and Westerblad, H. (1991). Force decline due to fatigue and intracellular acidification in isolated fibres from mouse skeletal muscle. *J. Physiol.* **434**, 307-322.

Lanza, I. R., Bhagra, S., Nair, K. S. and Port, J. D. (2011). Measurement of human skeletal muscle oxidative capacity by ³¹P-MR spectroscopy: a cross-validation with in vitro measurements. *J. Magn. Reson. Imag.* **34**, 1143-1150.

Larsson, N. G. and Oldfors, A. (2001). Mitochondrial myopathies. *Acta Physiol Scand* **171**, 385-393.

Larsson, N. G., Wang, J., Wilhelmsson, H., Oldfors, A., Rustin, P., Lewandoski, M., Barsh, G. S. and Clayton, D. A. (1998). Mitochondrial transcription factor A is necessary for mtDNA maintenance and embryogenesis in mice. *Nat Genet* **18**, 231-236.

Le Fur, Y., Nicoli, F., Guye, M., Confort-Gouny, S., Cozzone, P. J. and Kober, F. (2010). Grid-free interactive and automated data processing for MR chemical shift imaging data. *Magma* **23**, 23-30.

Matthews, P. M., Allaire, C., Shoubridge, E. A., Karpati, G., Carpenter, S. and Arnold, D. L. (1991). *In vivo* muscle magnetic resonance spectroscopy in the clinical investigation of mitochondrial disease. *Neurology* **41**, 114-120.

Milone, M. and Wong, L. J. (2013). Diagnosis of mitochondrial myopathies. *Mol. Genet. Metab.* **110**, 35-41.

Moggio, M., Colombo, I., Peverelli, L., Villa, L., Khani, R., Testolin, S., Di Mauro, S. and Sciacco, M. (2014). Mitochondrial disease heterogeneity: a prognostic challenge. *Acta Myol.* **33**, 86-93.

Moller, H. E., Kurlemann, G., Putzler, M., Wiedermann, D., Hilbich, T. and Fiedler, B. (2005). Magnetic resonance spectroscopy in patients with MELAS. *J. Neurol. Sci.* **229-230**, 131-139.

Moon, R. B. and Richards, J. H. (1973). Determination of intracellular pH by ³¹P magnetic resonance. *J. Biol. Chem.* **248**, 7276-7278.

Ogier, A., Sdika, M., Foure, A., Le Troter, A. and Bendahan, D. (2017). Individual muscle segmentation in MR images: A 3D propagation through 2D non-linear registration approaches. *Conf. Proc. IEEE. Eng. Med. Biol. Soc.* **2017**, 317-320.

Olsen, D. B., Langkilde, A. R., Orngreen, M. C., Rostrup, E., Schwartz, M. and Vissing, J. (2003). Muscle structural changes in mitochondrial myopathy relate to genotype. *J. Neurol.* **250**, 1328-1334.

Pariikh, S., Goldstein, A., Koenig, M. K., Scaglia, F., Enns, G. M., Saneto, R., Anselm, I., Cohen, B. H., Falk, M. J., Greene, C. et al. (2015). Diagnosis and management of mitochondrial disease: a consensus statement from the Mitochondrial Medicine Society. *Genet Med* **17**, 689-701.

Petty, R. K., Harding, A. E. and Morgan-Hughes, J. A. (1986). The clinical features of mitochondrial myopathy. *Brain* **109 (Pt 5)**, 915-938.

Place, N., Yamada, T., Bruton, J. D. and Westerblad, H. (2010). Muscle fatigue: from observations in humans to underlying mechanisms studied in intact single muscle fibres. *Eur J Appl Physiol* **110**, 1-15.

Radda, G. K., Bore, P. J., Gadian, D. G., Ross, B. D., Styles, P., Taylor, D. J. and Morgan-Hughes, J. (1982). ³¹P NMR examination of two patients with NADH-CoQ reductase deficiency. *Nature* **295**, 608-609.

Radda, G. K., Taylor, D. J. and Arnold, D. L. (1985). Investigation of human mitochondrial myopathies by phosphorus magnetic resonance spectroscopy. *Biochem Soc Trans* **13**, 654.

Rotig, A. and Munnich, A. (2003). Genetic features of mitochondrial respiratory chain disorders. *J. Am. Soc. Nephrol.* **14**, 2995-3007.

Santulli, G., Nakashima, R., Yuan, Q. and Marks, A. R. (2017). Intracellular calcium release channels: an update. *J. Physiol.* **595**, 3041-3051.

Scelsi, R. (1992). Morphometric analysis of skeletal muscle fibres and capillaries in mitochondrial myopathies. *Pathol. Res. Pract.* **188**, 607-611.

Shishmarev, D. (2020). Excitation-contraction coupling in skeletal muscle: recent progress and unanswered questions. *Biophys Rev* **12**, 143-153.

Szabadkai, G., Bianchi, K., Varnai, P., De Stefani, D., Wieckowski, M. R., Cavagna, D., Nagy, A. I., Balla, T. and Rizzuto, R. (2006). Chaperone-mediated coupling of endoplasmic reticulum and mitochondrial Ca²⁺ channels. *J. Cell Biol.* **175**, 901-911.

Taivassalo, T. and Haller, R. G. (2005). Exercise and training in mitochondrial myopathies. *Med. Sci. Sports Exerc.* **37**, 2094-2101.

Taivassalo, T., Jensen, T. D., Kennaway, N., DiMauro, S., Vissing, J. and Haller, R. G. (2003). The spectrum of exercise tolerance in mitochondrial myopathies: a study of 40 patients. *Brain* **126**, 413-423.

Tarnopolsky, M. A. (2016). Metabolic Myopathies. *Continuum (Minneap Minn)* **22**, 1829-1851.

Taylor, D. J., Kemp, G. J. and Radda, G. K. (1994). Bioenergetics of skeletal muscle in mitochondrial myopathy. *J. Neurol. Sci.* **127**, 198-206.

Theodorou, D. J., Theodorou, S. J. and Kakitsubata, Y. (2012). Skeletal muscle disease: patterns of MRI appearances. *Br J Radiol* **85**, e1298-1308.

Thorburn, D. R. (2004). Mitochondrial disorders: prevalence, myths and advances. *J. Inherit. Metab. Dis.* **27**, 349-362.

Tubbs, E. and Rieusset, J. (2016). Study of Endoplasmic Reticulum and Mitochondria Interactions by In Situ Proximity Ligation Assay in Fixed Cells. *J. Vis. Exp.*

Tubbs, E., Theurey, P., Vial, G., Bendridi, N., Bravard, A., Chauvin, M. A., Ji-Cao, J., Zoulim, F., Bartosch, B., Ovize, M. et al. (2014). Mitochondria-associated endoplasmic reticulum membrane (MAM) integrity is required for insulin signaling and is implicated in hepatic insulin resistance. *Diabetes* **63**, 3279-3294.

Vissing, J., Gansted, U. and Quistorff, B. (2001). Exercise intolerance in mitochondrial myopathy is not related to lactic acidosis. *Ann. Neurol.* **49**, 672-676.

Ward, S. R., Winters, T. M., O'Connor, S. M. and Lieber, R. L. (2020). Non-linear Scaling of Passive Mechanical Properties in Fibers, Bundles, Fascicles and Whole Rabbit Muscles. *Front. Physiol.* **11**, 211.

Westerblad, H. (2016). Acidosis Is Not a Significant Cause of Skeletal Muscle Fatigue. *Med. Sci. Sports Exerc.* **48**, 2339-2342.

Westerblad, H. and Allen, D. G. (1996). The effects of intracellular injections of phosphate on intracellular calcium and force in single fibres of mouse skeletal muscle. *Pflugers Arch.* **431**, 964-970.

Wieckowski, M. R., Giorgi, C., Lebedzinska, M., Duszynski, J. and Pinton, P. (2009). Isolation of mitochondria-associated membranes and mitochondria from animal tissues and cells. *Nat. Protoc.* **4**, 1582-1590.

Wredenberg, A., Wibom, R., Wilhelmsson, H., Graff, C., Wiener, H. H., Burden, S. J., Oldfors, A., Westerblad, H. and Larsson, N. G. (2002). Increased mitochondrial mass in mitochondrial myopathy mice. *Proc. Nat. Acad. Sci. U S A* **99**, 15066-15071.

Wu, F., Jeneson, J. A. and Beard, D. A. (2007). Oxidative ATP synthesis in skeletal muscle is controlled by substrate feedback. *Am. J. Physiol. Cell. Physiol.* **292**, C115-124.

Yamada, T., Ivarsson, N., Hernandez, A., Fahlstrom, A., Cheng, A. J., Zhang, S. J., Bruton, J. D., Ulfhake, B. and Westerblad, H. (2012). Impaired mitochondrial respiration and decreased fatigue resistance followed by severe muscle weakness in skeletal muscle of mitochondrial DNA mutator mice. *J. Physiol.* **590**, 6187-6197.

FIGURES

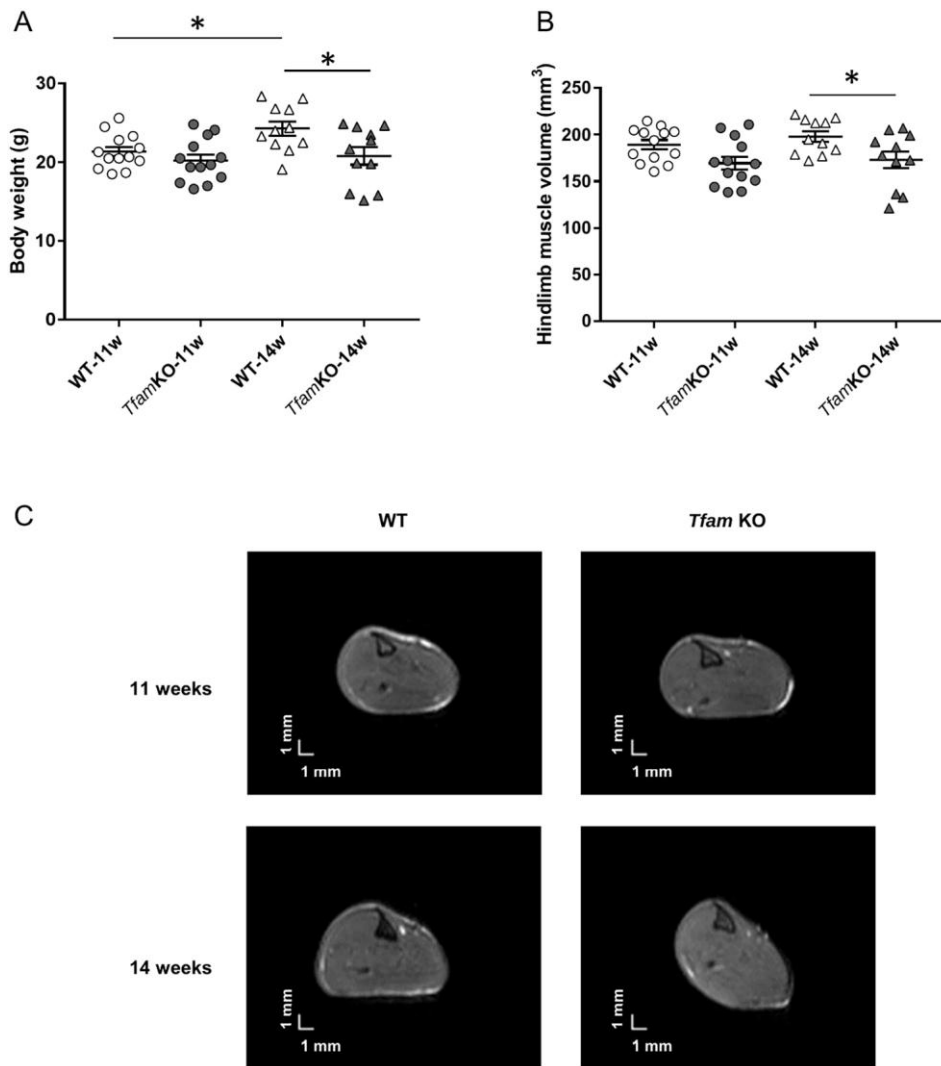


Fig. 1 *Tfam* KO mice presented a reduced body weight associated with muscle atrophy at 14 weeks. **A** Body mass in WT and *Tfam* KO mice. **B** Volume of hindlimb muscles in WT and *Tfam* KO mice. WT-11w, n=13; *Tfam* KO-11w, n=13; WT-14w, n=11; *Tfam* KO-14w, n=11. Data presented as individual values and mean±SEM. Significant difference * $P < 0.05$ (Two-way ANOVA and Sidak's post hoc test). **C** Representative axial MR images obtained from WT (left panels) and *Tfam* KO (right panels) at 11 weeks (top panels) and 14 weeks (bottom panels).

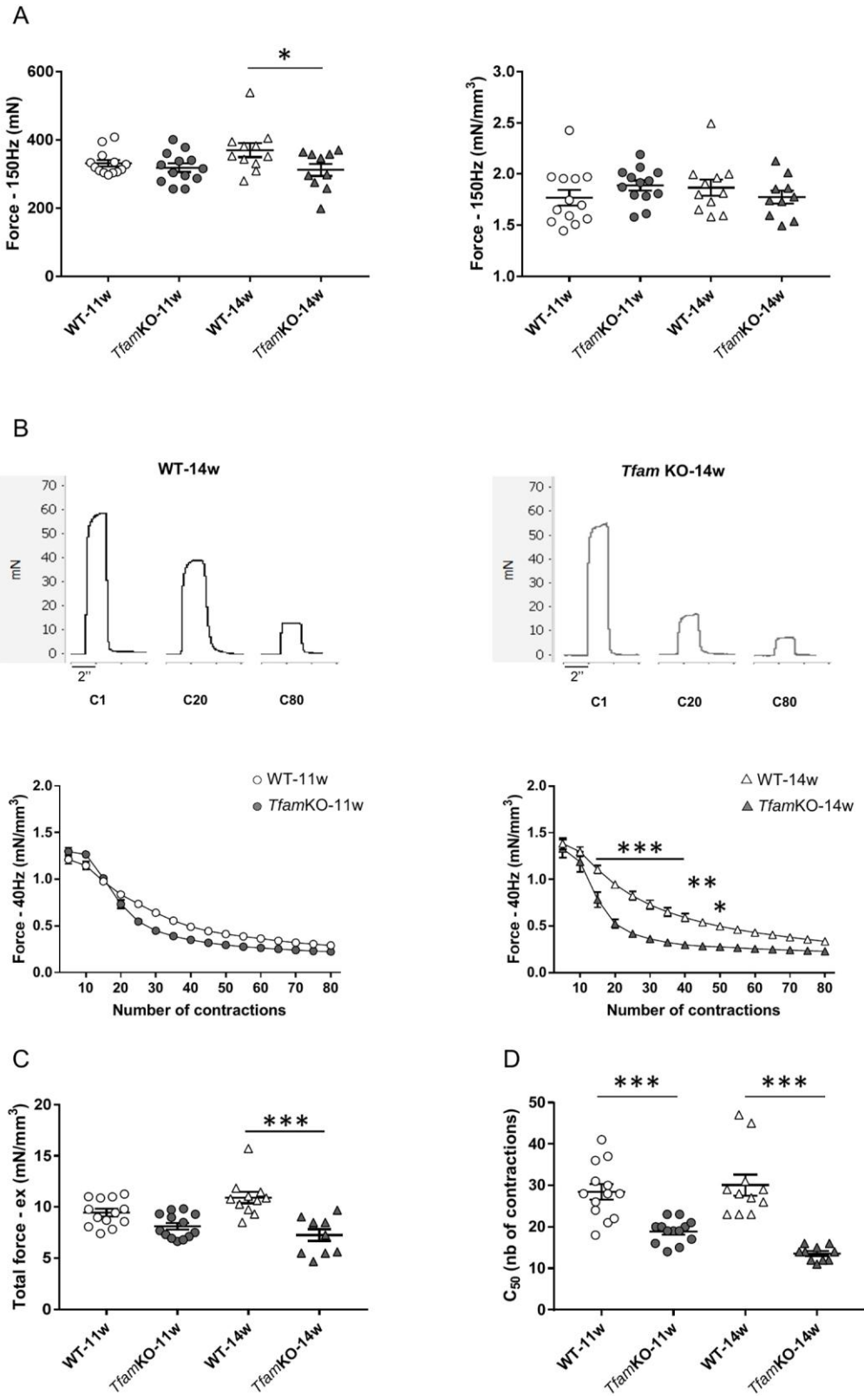


Fig. 2 *Tfam* deletion resulted in accelerated muscle fatigue in mice at 11 and 14 weeks and muscle weakness only at 14 weeks. **A** Maximal (150 Hz) absolute (left panel) and specific (right panel) force of the plantar flexor muscles *in vivo*. **B** Representative force traces of the plantar flexor muscles in WT and *Tfam* KO mice at 14 weeks recorded during the 1st contraction (C1), 20th contraction (C20), last contraction (C80) of the 80 contractions of fatiguing stimulation (top panels) and average data of *in vivo* specific force (bottom panels). **C** Total specific force of the plantar flexor muscles produced during the whole fatiguing protocol. **D** Contraction at which force production was 50% of the unfatigued force (C_{50}). WT-11w, n=13; *Tfam* KO-11w, n=13; WT-14w, n=11; *Tfam* KO-14w, n=10. Data presented as individual values and mean \pm SEM for panels A and C. Values are mean \pm SEM for panel B. Significant difference *, ** and *** $P<0.05$, $P<0.01$ and 0.001, respectively. Two-way ANOVA with repeated measures on contraction number and Tukey's post hoc test for force during exercise; two-way ANOVA for all other comparisons with Sidak's post hoc test for absolute force and Tukey's post hoc for total force and C_{50} . No significant difference between all groups was found for normalized force at 150 Hz with two-way ANOVA.

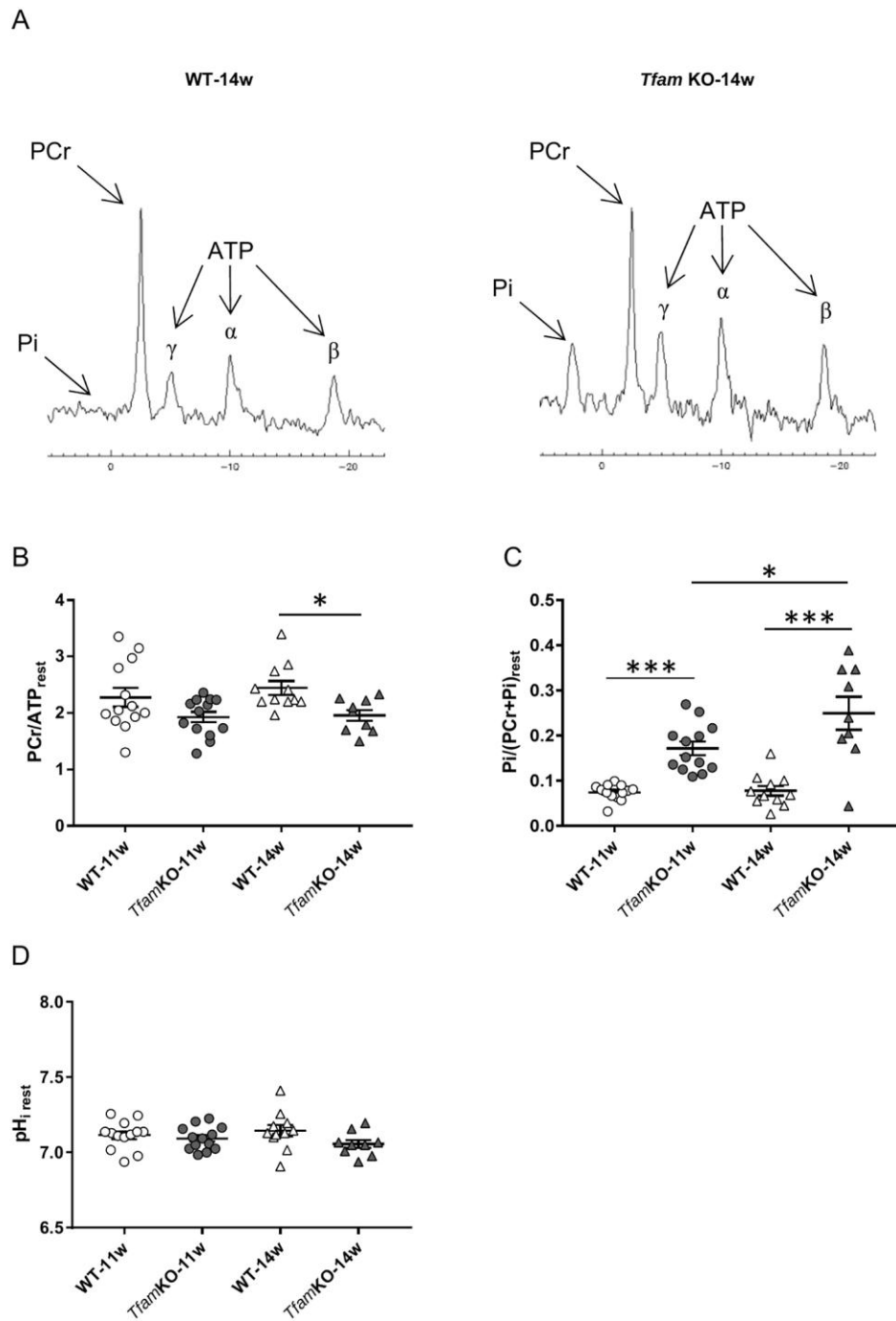


Fig. 3 Metabolic parameters at rest were altered in *Tfam* KO mice and progressed between 11 and 14 weeks. A Example of resting ^{31}P -MR spectra in WT and *Tfam* KO muscles at 14 weeks. Phosphocreatine (B), inorganic phosphate (C), and pH_i (D) measured at rest. WT-11w, $n=13$; *Tfam* KO-11w, $n=13$; WT-14w, $n=11$; *Tfam* KO-14w, $n=9$. Data presented as individual values and mean \pm SEM. Significant difference * and *** $P<0.05$ and

0.001, respectively (two-way ANOVA with Sidak's post hoc test for $\text{PCr}/\text{ATP}_{\text{rest}}$ and Tuckey's post hoc for $\text{Pi}/(\text{PCr}+\text{Pi})_{\text{rest}}$; no significant difference was found for $\text{pH}_{\text{i rest}}$ with two-way ANOVA.). PCr: phosphocreatine; Pi: inorganic phosphate; ATP: adenosine triphosphate; pH_{i} : intracellular pH.

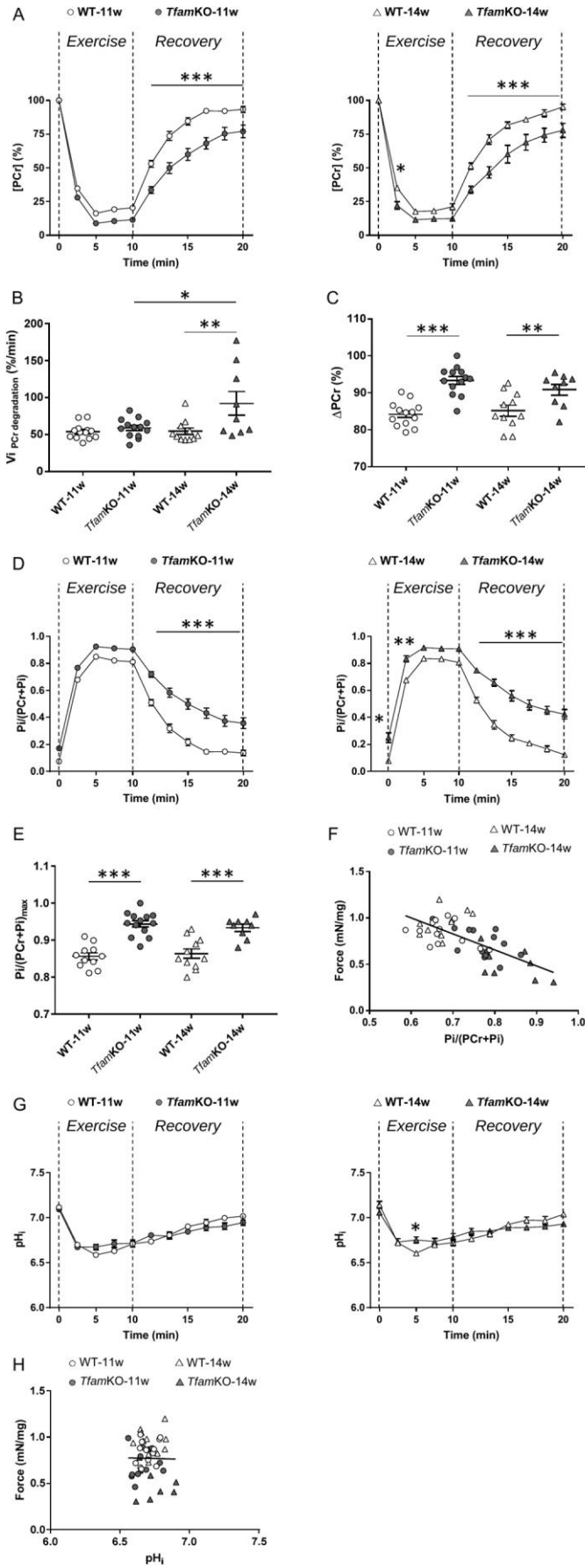


Fig. 4 Impaired phosphocreatine and inorganic phosphate metabolism during exercise in *Tfam* KO mice. **A** [Phosphocreatine] levels throughout the stimulation period and during the recovery after the stimulation. **B** Initial rate of [phosphocreatine] degradation and **C** total magnitude of [phosphocreatine] reduction during the stimulation period. **D** [Inorganic phosphate] levels during fatiguing stimulation and recovery. **E** Maximal inorganic phosphate reached during fatiguing protocol. **F** Relationship between force and inorganic phosphate after 2.5 min of fatiguing exercise ($r=-0.69$; $P<0.001$). **G** pH_i during stimulation and recovery periods. **H** Relationship between force and pH_i after 2.5 min of fatiguing exercise ($r=-0.01$; $P=0.93$). WT-11w, $n=13$; *Tfam* KO-11w, $n=13$; WT-14w, $n=11$; *Tfam* KO-14w, $n=9$. Values are mean \pm SEM for panels A, D and G. Data presented as individual values and mean \pm SEM for other panels. Significant difference *, ** and *** $P<0.05$, 0.01 and 0.001, respectively (two-way ANOVA with repeated measures on time and Tukey's post hoc test for time-course of phosphocreatine, inorganic phosphate and pH_i ; two-way ANOVA for all other comparisons except linear regressions with Sidak's post hoc test for ΔPCr and $Pi/(PCr+Pi)_{max}$ and Tukey's post hoc for $Vi_{PCr\ degradation}$). PCr: phosphocreatine; Pi: inorganic phosphate; $Vi_{PCr\ degradation}$: initial rate of phosphocreatine breakdown; pH_i : intracellular pH.

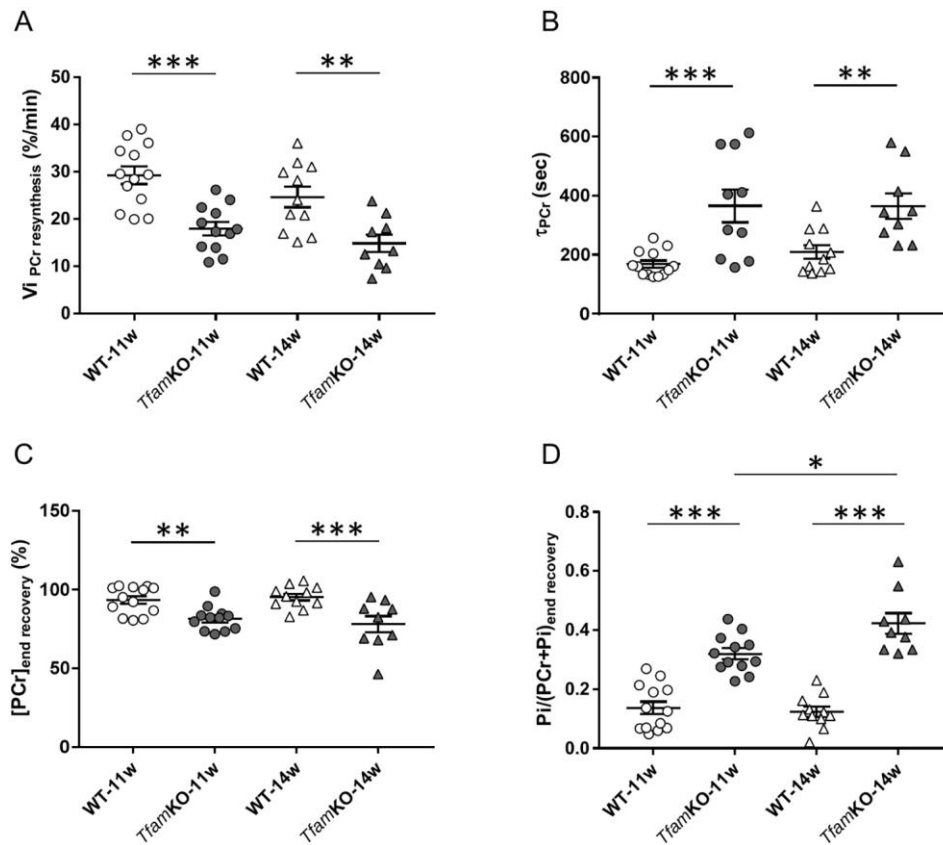


Fig. 5 Slowed recovery of metabolites implies decreased mitochondrial oxidative capacity in 11 and 14 weeks old *Tfam* KO mice. **A** Initial rate of phosphocreatine resynthesis after the stimulation bout. **B** Time constant of [phosphocreatine] recovery during the 10 min recovery phase after exercise. **C** [Phosphocreatine] at the end of the recovery period. **D** [Inorganic phosphate] at the end of the 10 min recovery period. WT-11w, n=13; *Tfam* KO-11w, n=12 for all analyses except for $T_{\text{Phosphocreatine}}$ for which n=10; WT-14w, n=11; *Tfam* KO-14w, n=9. Data presented as individual values and mean \pm SEM. Significant difference *, ** and *** $P < 0.05$, 0.01 and 0.001, respectively (two-way ANOVA with Tukey's post hoc test for $\text{Pi}/(\text{PCr}+\text{Pi})_{\text{end recovery}}$ and Sidak's post hoc for all other comparisons). PCr: phosphocreatine; Pi: inorganic phosphate; $V_i \text{ PCr resynthesis}$: initial rate of phosphocreatine resynthesis; T_{PCr} : time constant of [phosphocreatine] recovery.

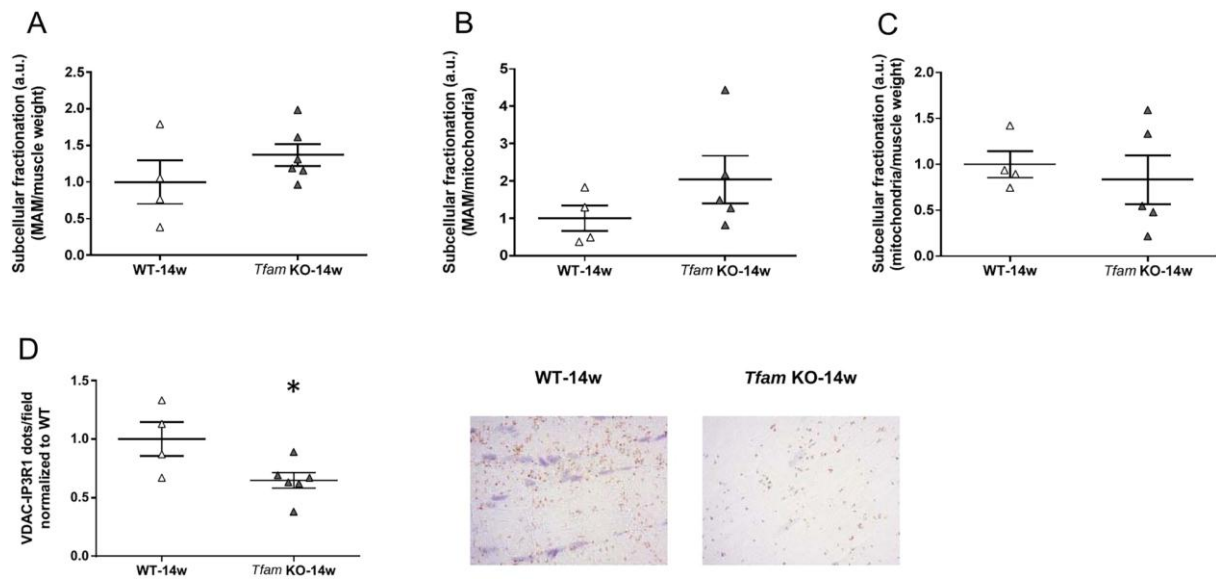


Fig. 6 *Tfam* KO mice showed decreased interaction points between sarcoplasmic reticulum and mitochondria. Quantification of the normalized protein ratio of MAM over muscle weight (A) and over pure mitochondria (B) from gastrocnemius muscle fractionation. C Quantification of the normalized protein ratio of mitochondria over muscle weight from gastrocnemius muscle fractionation in *Tfam* KO and WT mice. D Quantitative analysis of VDAC1-IP3R1 interactions (left panel) and representative images of the VDAC1-IP3R1 interactions (brown dots) measured by *in situ* PLA in paraffin-embedded gastrocnemius muscle of in WT (top right panel) and in *Tfam* KO mice (bottom right panel). Data presented as individual values and mean \pm SEM and normalized to the mean value in WT muscles, which was set to 1.0. Significant difference * $P < 0.05$. Unpaired Mann-Whitney test for MAM. Unpaired t-test for VDAC-IP3R1. MAM: mitochondria-associated membranes.

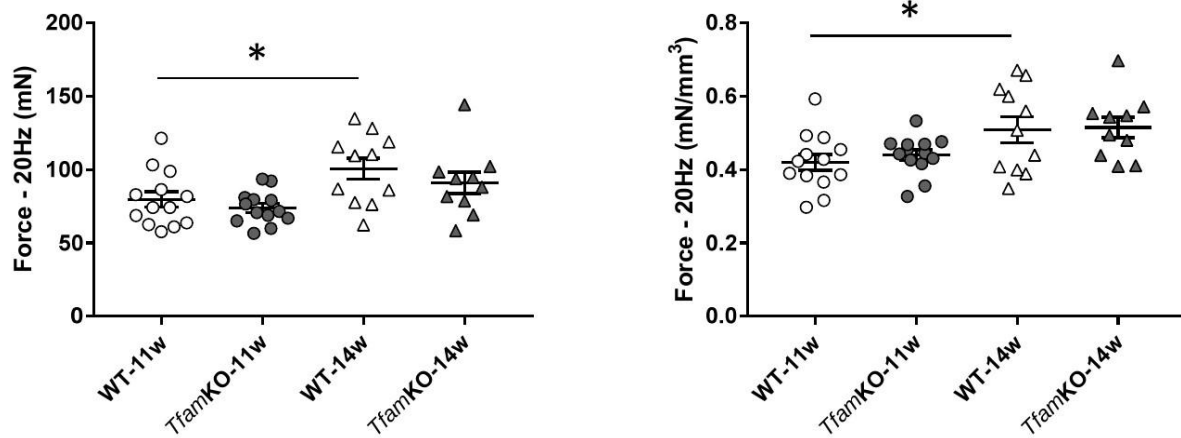


Fig. S1. Absolute and specific submaximal forces in the unfatigued state were unaltered in *Tfam* KO mice. Absolute (left panels) and specific (right panels) force production in response to 20 Hz stimulation. WT-11w, n=13; *Tfam* KO-11w, n=13; WT-14w, n=11; *Tfam* KO-14w, n=10. Data presented as individual values and mean±SEM. Significant difference *, $P < 0.05$ (Two-way ANOVA with Sidak's post hoc test).

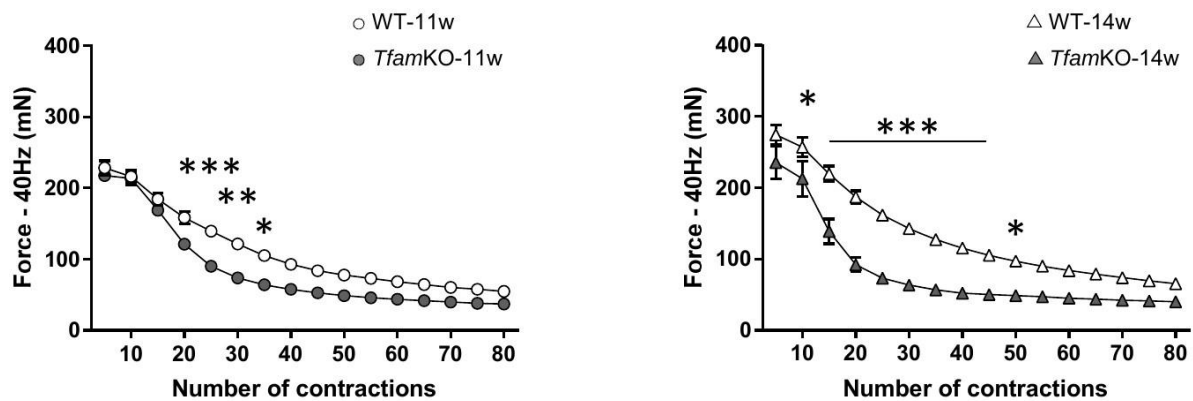


Fig. S2. Absolute force decreased more rapidly during exercise in *Tfam* KO mice. *In vivo* absolute force of the plantar flexor muscles during the fatiguing stimulation protocol at 11 weeks (left panel) and 14 weeks (right panel) in WT and *Tfam* KO mice. WT-11w, n=13; *Tfam* KO-11w, n=13; WT-14w, n=11; *Tfam* KO-14w, n=10. Values are mean±SEM. Significant difference *, ** and *** $P < 0.05$, 0.01 and 0.001, respectively (two-way ANOVA with repeated measures on contraction number and Tuckey's post hoc test).

Table S1. Metabolites at rest and at the end of the 10 min recovery period post-exercise in WT and *Tfam* KO mice.

Metabolites	11 weeks		14 weeks	
	WT	<i>Tfam</i> KO	WT	<i>Tfam</i> KO
[PCr]_{rest} (%)	100	100	100	100
[PCr]_{end recovery} (%)	93±2	81±2*** ##	95±2	78±5*** ###
Pi/(PCr+Pi)_{rest}	0.07±0.01	0.17±0.01	0.08±0.01	0.25±0.04
Pi/(PCr+Pi)_{end recovery}	0.14±0.02	0.32±0.02*** ### \$	0.12±0.02	0.42±0.04*** ### \$\$

WT-11w, n=13; *Tfam* KO-11w, n=13; WT-14w, n=11; *Tfam* KO-14w, n=9. Values are mean±SEM. Significantly different from rest (same age and same genotype) * and *** $P<0.05$ and 0.001, respectively. Significant difference between genotypes (same age and same condition) ## and ###, $P<0.01$ and 0.001, respectively. Significant difference between ages (same genotype and same condition) \$ $P<0.05$. One-way ANOVA and Tukey's post hoc test for all comparisons. PCr: phosphocreatine; Pi: inorganic phosphate.